ORIGINAL ARTICLE

Multi-layer solid-state ultrasonic additive manufacturing of aluminum/copper: local properties and texture

Alireza Behvar[1] · Shawkat I. Shakil[1] · Hadi Pirgazi[2] · Mark Norfolk[3] · Meysam Haghshenas[1]

Abstract

Ultrasonic additive manufacturing (UAM) is an advanced joining technique that utilizes ultrasonic vibrations to bond layers of metal foil together. UAM offers several benefits over traditional manufacturing methods, including enhanced design flexibility and reduced material waste, and its potential applications in various industries such as aerospace, automotive, and biomedical engineering are being actively explored. The study employs a nanoindentation apparatus to investigate the effect of the UAM process on the local mechanical properties of the bonded interface, along with changes in microstructure, which were investigated using scanning electron microscopy and electron back-scattered diffraction. The results revealed a significant correlation between material hardness and local plasticity. EBSD has revealed that the grain size distribution of Al far from the interface contains 57% of the grains less than 3 μm in size, while at the interface this number rises to approximately 78%, indicating that the average grain size decreases as it approaches the interface. This result is consistent with nanoindentation results that demonstrated a gradual change in the hardness of Al foil far from the interface to close to the interface (the maximum penetration depth near the interface was 500 nm less than far from the interface). Both EBSD and nanoindentation disclose the effect of work hardening close to the interface, which is related to dislocation accumulation with a density of 8.6×10^{-10} cm^{-2} beneath the interface. The consistency of hardness and Young's modulus with the pole figures and microscopic images demonstrated that plasticity flow and fine grain distribution would only occur in the vicinity of the interface in the softer metal region. Although the harder metal did not exhibit plasticity or recrystallization, the hardness, and Young's modulus map indicated the formation of a layer of small grains close to the interface on the aluminum side owing to strain hardening and dynamic recrystallization.

1 Introduction

1.1 Ultrasonic additive manufacturing (UAM) technique

Ultrasonic additive manufacturing (UAM) is a technique that employs ultrasonic energy and pressure to generate oscillating shear strain between the faying surfaces and produces a metallurgical bond [1–3]. The UAM process, initially developed by White in 2003 [4, 5], is the method for fabricating a three-dimensional metal component by alternating additive and subtractive processes.

For the UAM of metallic materials in solid state, two fundamental conditions must be met: (i) generation of clean surfaces at the atomic scale with no barrier layers and (ii) nascent metal-to-metal contact between these clean surfaces [6]. Due to friction and shear deformation at the interface caused by ultrasonic vibration, microscale metallurgical bonding could be formed [7]. During additive operations, thin foil tape layers ($\sim 150 \mu$m) are joined with one another on a substrate via a solid-state technique that employs ultrasonic oscillations (20 kHz) at high strain rates (up to 10^5 s^{-1}) without melting the layers. The ultrasonic vibrations are applied via a sonotrode, which is a cylindrical rolling horn [8]. Down force and ultrasonic oscillations both contribute

✉ Meysam Haghshenas
  meysam.haghshenas@utoledo.edu

1 Department of Mechanical, Industrial, and Manufacturing Engineering, University of Toledo, Toledo, OH, USA

2 Department of Electromechanical, Systems and Metal Engineering, Ghent University, Ghent, Belgium

3 Fabrisonic LLC, Lewis Center, OH, USA

to the plastic flow of the material, as well as the destruction and redistribution of surface oxide layers and impurities, hence facilitating a clean mating surface for solid joints [9, 10]. As it moves ahead, the sonotrode simultaneously exerts a downward pull on the foil (in the z-direction) and scrapes laterally (in the y-direction) (Fig. 1a, b). The sonotrode's ultrasonic vibrations cause the localized surface asperities to bend plastically and the surface oxides at the interface of the foils to disintegrate. This process produces two surfaces that are atomically pristine and adhere at temperatures much below their respective melting points (the layer-by-layer Al6061-Cu110 foils depicted in Fig. 1c are the actual manufactured part for this study which is produced by the UAM method) [8, 11].

The comparatively brief fabrication durations and moderate processing temperatures offer several advantages to this kind of production, such as versatility (producing composites by layer-by-layer process), low heat input (does not need high temperature for bonding), repairability (easy repair of damaged part), and the capability to engineer materials with directional properties. UAM has been utilized for purposes such as joining dissimilar or difficult-to-weld metals [12, 13] and embedding fragile materials such as ceramics or sensors [8, 14]. Typically, when dissimilar metallic foils are bonded together by UAM, a bilayer consolidation strategy consisting of a harder foil on top of a softer foil is utilized [15, 16]. It has been demonstrated [7, 17] that the softer foil can be severely deformed to have a large area of intimate contact with the harder foil and to occupy the surface micro-valleys of the harder foil. Because the harder foil makes direct contact with the sonotrode and engraves a coarser surface, the roughness of the surfaces of the harder foil that make direct

Fig. 1 Schematic representation of the UAM process. **a** The action of the sonotrode exerting a downward force on the foil and scraping laterally. **b** The result of this process, where surface asperities bend plastically and surface oxides disintegrate, producing atomically pristine surfaces that adhere at temperatures below their melting points. **c** A real manufactured part and the layer-by-layer bonded Al6061/Cu110 foils via the UAM process
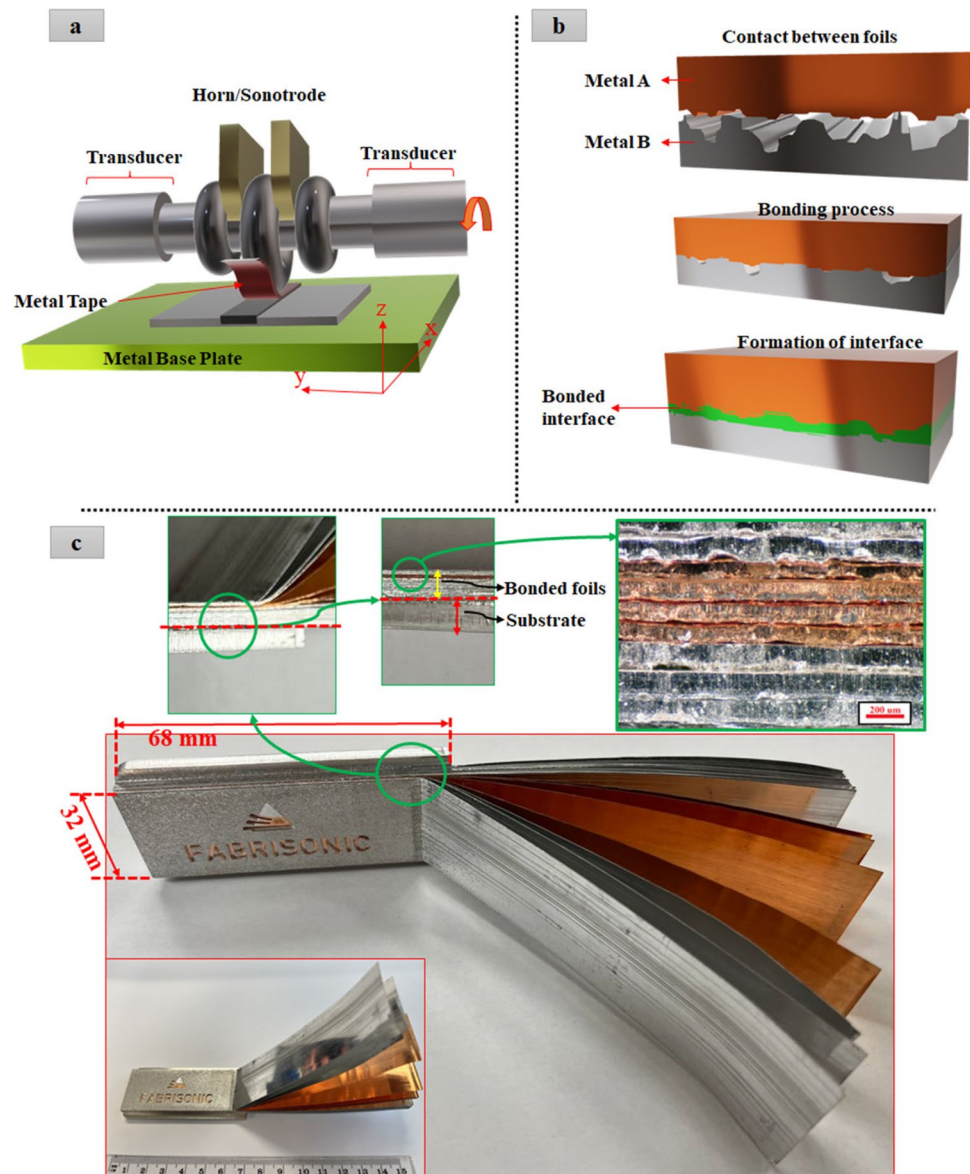
contact with the upper and lower surfaces of the soft foil during consolidation is significantly different. Consequently, the two surfaces of the soft foil experienced varying degrees of deformation, and two varieties of interfaces can be formed. The difference in interfacial texture and bonding hardness between the two types of interfaces between dissimilar metals have received little attention at this point.

Figure 2 shows the side view of the UAM machine, and the ultrasonic horn which can have a textured surface to engage the metal foil. Ultrasonic vibrations, generated by transducers attached to the sonotrode, scrub the foil against the substrate (much like friction welding), creating a solid-state (no melting) bond between the metal foil and lower substrate, i.e., baseplate or previous foil.

Important UAM mechanisms include oxide fracture under pressure and plastic deformation of surface asperities via shear [18]. Oxide dispersion permits nascent metal surfaces to interact and form metallic connections, whereas surface asperity deformation promotes dynamic recrystallization of the interface microstructure [19, 20]. The result is a limited weld zone on the order of 10–20 μm in width with bulk temperatures far below the melting point of the metal [21]. It is commonly accepted that localized slip and sublayer plastic deformation are desired, and that interfacial slip is responsible for breaking down surface oxides, allowing nascent metal interaction at asperity contact points. As plastic deformation of asperities is one of the primary mechanisms of the UAM process, it is more difficult to treat tougher materials because they require more energy to deform and collapse surface asperities. High oscillation amplitude and/or normal force will be necessary to attain a high bonding density [9, 10]. In addition, certain material combinations, particularly

Fig. 2 The UAM machine. **a** Side view. **b** Close view of the ultrasonic horns
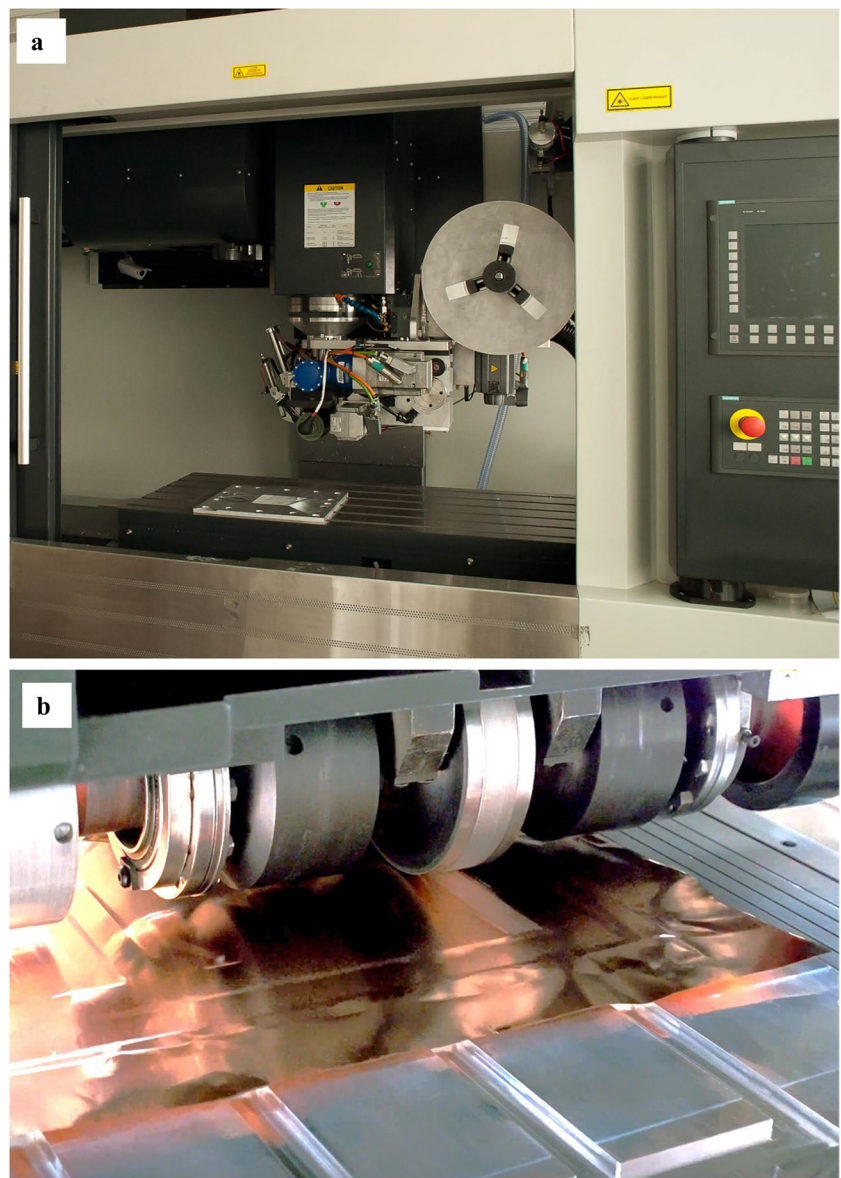
those involving pure metals, are hampered by oxide layer interference. UAM exhibits mechanical strength anisotropy based on the build direction and resulting layer orientation, a characteristic shared by most AM processes. Post-process heat treatments that boost bonding strength through the controlled formation of intermetallic compounds or the relaxing of residual stresses and promotion of inter-diffusion [2, 10] can reduce anisotropies.

1.2 Literature review and objectives of the present research

Since UAM is a low-temperature technique, it is advantageous for joining dissimilar metals that tend to create intermetallic [15]. As a result, a variety of dissimilar metals, including Al–Ti [15, 22–24], Al–Cu [8, 19, 25], Al–Ni [26, 27], and Steel–Ta [17], were joined using the UAM technique. Cu/Al laminate metal composites (LMCs) were increasingly utilized in modern engineering due to their superior thermal conductivity, electroconductivity, impedance, and corrosion resistance [28]. However, it has been reported that fusion welding Al and Cu is challenging due to the formation of intermetallic compounds at the interface, necessitating the use of solid-state welding techniques [29, 30]. In a study, Johnson et al. [31] cast doubt on the idea of oxide fracture and dispersion, samples of Aluminum 3003 were analyzed using a scanning electron microscope/focused ion beam (SEM/FIB) instrument to generate ion beam-induced secondary electron micrographs (IBISEMs). A persistent surface oxide layer existed between the welded foils, according to the results of this approach. It was postulated that mechanical interlocking and bonding between aluminum and Al_2O_3 were responsible for bond formation in UAM structures [25, 31]. Many obstacles must be overcome before aluminum and copper can be bonded successfully. Above 120 °C, intermetallic compounds can occur between aluminum and copper, and these compounds often have low strength, brittleness, and high electrical resistance [32]. Therefore, joining aluminum and copper by fusion welding methods is very challenging [33, 34]. Because of the need to avoid the liquid phase when joining these materials, solid-state methods are an obvious choice. However, there are solid-state processes that can generate intermetallic at the interface without exceeding the melting point, even if they operate at much higher temperatures. Few studies [8, 25, 34] have attempted to join aluminum and copper using UAM. Using transmission electron microscopy (TEM), Sietins et al. [35] identified the concentration profile and Al–Cu compounds for a Cu/Al LMC fabricated by UAM. Later, Fujii et al. [36] reported that in the vicinity of the Cu/Al interface bonded by ultrasonic welding, severe shear deformation occurred parallel to ultrasonic oscillations. Particularly, Zhou et al. [7] investigated the diffusion and

intermetallic phase formation at the interface of Al/Cu, as well as the recrystallization phenomena caused by the distribution of shear stress at the interface. Using Al3003 and Cu110, Ram et al. [34] conducted a feasibility study on the UAM effect on intermetallic phase formation. The SEM micrographs revealed an interface that seemed "tight" at low magnification and a thin porous layer on the aluminum side at high magnification [34]. Notably, the intermetallic formation was not seen in images of the interface captured by the backscatter electron detector. In another study, Sietins et al. [35, 37] reported a very thin layer (less than 10 μm) of intermetallic phases at the interface of bonded materials. This result implies that UAM could bond foils at temperatures low enough to inhibit brittle intermetallic development.

The study focuses on the UAM process of joining Al6061-H18 and Cu-110 foils, which are traditionally challenging metals to join. By examining the mechanical properties and microstructural changes in this specific combination, the study expands the understanding of UAM's applicability to difficult-to-join metal combinations. Considering the need for investigating the mechanical properties at the interface and layers (e.g., Al and Cu layers) of the composite structure, conventional mechanical tests (e.g., tensile testing) would not be feasible; rather a small-scale mechanical testing (e.g., depth sensing nanoindentation testing) would be very effective in assessing the location-dependent mechanical properties. Based on the literature review, the UAM-produced Al-Cu structures are less explored and there is no study on the assessment of their local mechanical properties like hardness and Young's modulus (e.g., variation in properties along interface and layers) and associated microstructure-property correlation. In this regard, the UAM process has been used to produce an additively manufactured layered composite of Al6061-Cu110 at room temperature, and the depth-sensing nanoindentation technique along with electron backscatter diffraction (EBSD) assessments was utilized to study the location-based mechanical properties, microstructure, and texture. The effect of the UAM process on dynamic recrystallization in the welded interface has also been studied.

2 Experimental procedure

On an Al6061-T451 substrate, bilayers of 150 μm thick Al6061-H18 printed foils and half-hard printed foils Cu-110 were ultrasonically bonded (the graphical demonstration of the experimental procedure is illustrated in Fig. 3). The UAM system with subtractive milling capabilities was utilized for the construction. Fabrication parameters included a welding force of 3500 N, a welding speed of 25.4 mm/s, and a vibration amplitude of 41.55 μm. During deposition, the substrate was preheated to 50 °C,
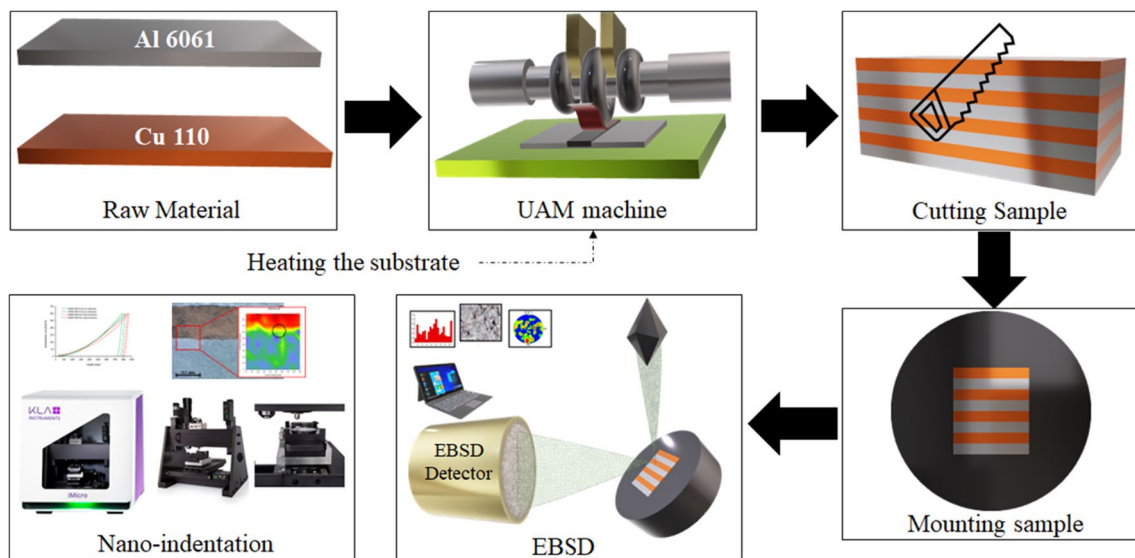
Fig. 3 Graphical demonstration of the experimental procedure, beginning with raw material to final EBSD and nano-indentation tests

as this has been demonstrated to improve plastic flow and adhesion [6, 38]. The samples were then mounted and sectioned along the plane of vibration of the sonotrode for metallographic analysis. Care was taken to guarantee adequate coolant flow during sectioning to preserve interface microstructures. The samples were mounted in epoxy at room temperature and then polished with grinding paper (1200 grit), followed by diamond polishing with 6, 3, and 1 μm diamond slurries. Using a Buehler Vibrometer and a colloidal silica suspension with a particle size of 0.05 microns for 4.5 h, the deformation zone from previous polishing stages was removed. A Leica DM 750P microscope was utilized for optical microscopic investigations. EBSD measurements were carried out to investigate the microstructural characteristics of the bonded structure, focusing particularly on the aluminum and copper foils as well as at the interfaces between aluminum/copper and aluminum/substrate (as shown in Fig. 3a). To conduct these measurements, a state-of-the-art FEI Quanta™ 450 field emission gun scanning electron microscope (FEG-SEM) was utilized. This high-resolution instrument enabled us to capture detailed images and data across specific regions of interest in our samples. EBSD investigation focused on specific regions sized 120 μm by 120 μm on the cross-sections of the bonded structure. Two distinct step sizes, 60 nm, and 200 nm were used to generate the EBSD maps. The choice of these step sizes ensured an optimal balance between spatial resolution and the area of coverage, thus facilitating a comprehensive understanding of the microstructural details across the interfaces and within the foils. The EBSD data

was collected and post-processed using EDAX TSL data collection and analysis software.

For small-scale mechanical characterization, a depth-sensing nanoindentation testing technique was employed. The nanoindentation system (iMicro Nanoindenter manufactured by KLA Instruments, USA) is equipped with a self-similar three-sided diamond Berkovich indenter with a tip radius of 100 nm. Load-controlled indentation tests (peak load of 300 mN, and a loading/unloading rate of 10 mN/s with 5 s dwell time), ISO 14557 standard [39], and high-speed hardness mapping were conducted on the cross-section of the multi-layered printed structure. The indentation hardness and modulus were then calculated according to the Oliver-Pharr method [40]. The nanoindentation system's continuous stiffness measurement (CSM) technique enabled direct measurement of dynamic contact stiffness during an indentation test's loading phase, enabling precise monitoring of small-volume deformation. To reduce error in indentation depth or displacement, thermal drift was also limited to 0.10 nm/s throughout each test. Indents were also carefully positioned with sufficient space between them to prevent any plastic domain overlap between neighboring indents. Furthermore, before running the tests, the test system was carefully calibrated using a reference material (fused silica) to ensure the repeatability of the results. To study the variation of mechanical properties at the interface, high-speed hardness mapping was also performed at the interface area between the Al and Cu layers employing an indentation load of 100 mN. A 10×10 array of indents was performed over an area of 300×300 μm^2.

3 Results and discussion

3.1 UAM's multilayer arrangement

Figure 4a presents a simplified schematic of the multilayer structure. The micrograph in Fig. 4b shows the bilayer configuration of Al and Cu foils along with the substrate. The magnified location in Fig. 4b shows that plastic flow occurs most strongly near the crests and troughs found on the upper surface of the Cu layer. This is because the sonotrode touches the build's top surface, causing localized "trough" and "crest" formations through heat generation by friction. Since Al is softer than Cu, it follows the shape of the interface and undergoes considerable plastic flow there (as marked by the red arrows in Fig. 4b). The thin region of the interface is found as a dark line in the high-magnification SEM image in Fig. 4b, and it will be analyzed by EBSD in the following section. Additionally, understanding the process of bond formation requires first looking at how deformation affects the crystallographic grain structure which needs to be analyzed by EBSD assessments.

Following Truog et al.'s research [25] and the Al-Cu phase diagram [41], intermetallic phases can form during the UAM process due to local temperature rises. Truog et al. [25] and Ikeda et al. [42] reported the formation of $CuAl_2$, $CuAl$, and Cu_9Al_4 intermetallic thin layers with a thickness of less than 1 µm at the Al-Cu interface boundary. Also, according to the findings of Zhou et al. [7] and Pagan et al. [8] on Al-Cu UAM, copper composition in the interface was a function of diffusion distance (like Fick's diffusion law) and a very thin layer of intermetallic structures was observed. However, referring to the experimental procedure, the UAM has been conducted at room temperature; consequently, significant temperature-dependent phenomena in this process cannot be anticipated.

3.2 Electron backscatter diffraction (EBSD) assessments

3.2.1 Characterization of Al-substrate interface microstructure

The EBSD inverse pole figure (IPF) map (Fig. 5a, b) of the Al-substrate interface (the region of scan 1 in Fig. 4a) reveals significant plastic deformation and recrystallization near the interface in the Al6061 region. Since the substrate is preheated cast aluminum, the grain size is much larger than that of the Al6061 foil, and it should be harder. During sonotrode movement, the friction and force effect on the strong substrate caused deformation in the bottom of the Al6061 foil (which is softer than the substrate), therefore it appears that only the Al6061 foil underwent dynamic recrystallization close to the interface. As a result of local plasticity, the primary mechanism of the UAM process, the general trend of grain orientation demonstrates a small mass flow that has been shown with black arrows in Fig. 5b.

As depicted in Fig. 5a, the morphological orientation of the grains in an Al6061 foil 3D-printed part is horizontal (aligned with the direction of printer movement), despite the presence of significant dynamic recrystallization near the bonding interface. The magnified IPF image presented in Fig. 5b reveals a noticeable directional preference in the reorganization of grains. This phenomenon may stem from the substrate metal's greater hardness and resistance to deformation, which forces the plastic flow in the upper layer to divert from the substrate (meaning the upper layer's
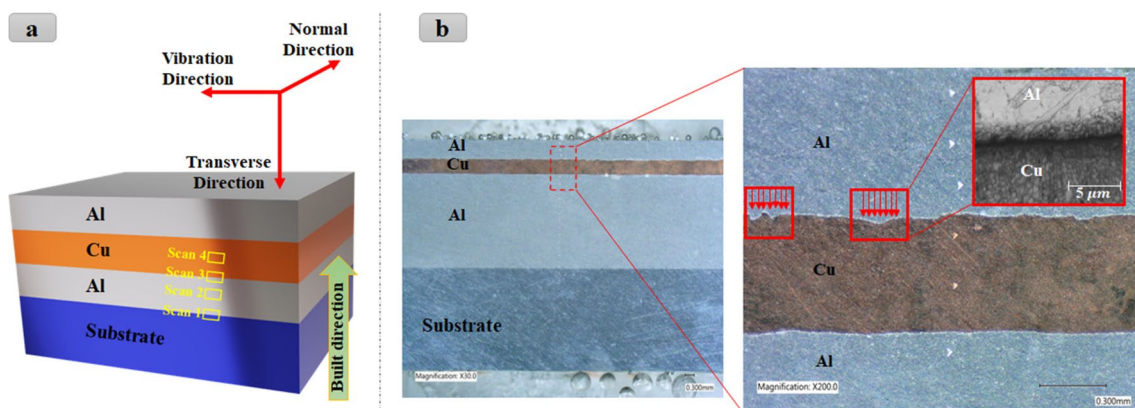

Fig. 4 **a** The schematic of the multilayer arrangement of the UAM technique used to fabricate the sample. **b** An optical micrograph of the UAM sample with some trough and crest in the Al-Cu interface and Al flow through the boundary. Note: The regions where the Al6061 flowed into the asperities created in the Cu110 by the sonotrode
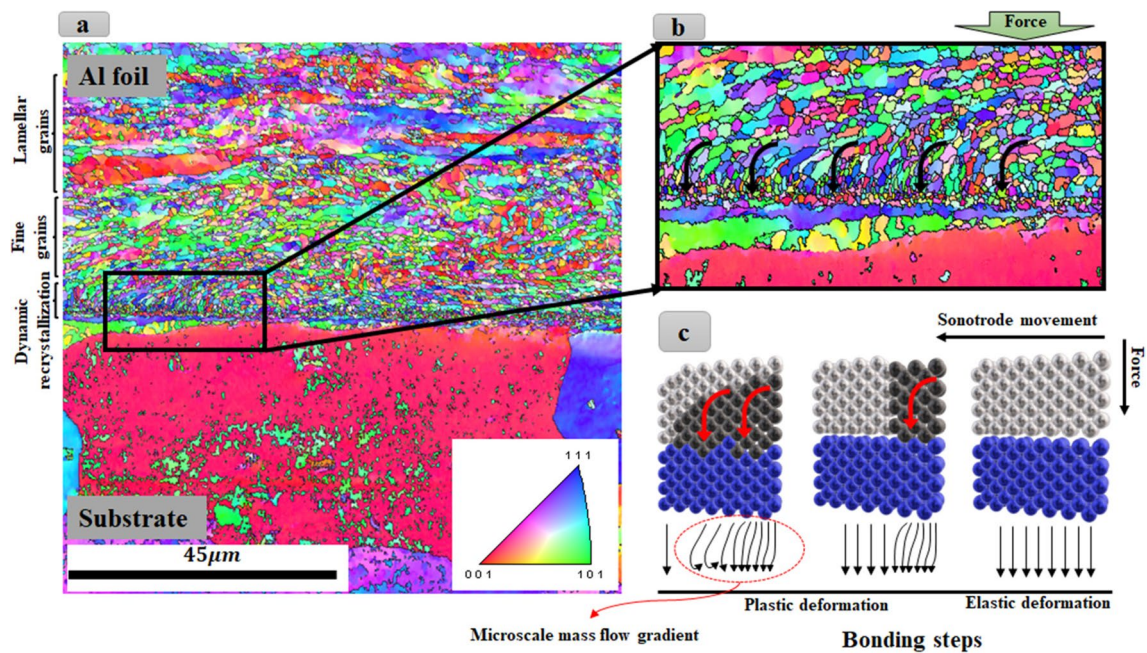
Fig. 5 **a** IPF of Al6061- substrate interface in scan 1 region of Fig. 4a. **b** The zoom-in of interface and plasticity trendline marks. **c** Schematic of atomic scale local deformation and bonding process through the UAM and plasticity flow marks near the interface, as it seems due to sonotrode movement the cyclic deformation in microscale causes (black area) atomic diffusion through the other metal, the black arrow is showing the mass flow gradient which is in consistency with EBSD of the interface

plastic flow is unable to penetrate the substrate). In the process of local plastic deformation, interactions between twins, slipping bands, and the robust surface of the substrate could occur. The in-process deformation and temperature lead to the reorganization of dislocations to low energy structures, formation of sub-grains and ultimately trigger recrystallization. The effect of substrate interface resistivity on the deformation process is evident in Fig. 5b. The black arrows in Fig. 5b and the schematic in Fig. 5c illustrate the local plastic flow trendline marks that have resulted in grain orientation near the interface.

3.2.2 Characterization of Al and Cu foils microstructure

Figure 6 demonstrates the EBSD-IPF and pole figure of both aluminum and copper printed foils following the UAM process. Referring to this figure, these two materials have a preferred distribution of grain orientation; in the aluminum foil's pole figure map (Fig. 6a), there is an orientation tendency toward the < 111 > direction. The SEM and IPF images of aluminum in Fig. 6a reveal a microstructure with numerous small-size grains dispersed throughout the entire microstructure. This would be the result of the printing process and subsequent thermal treatment, which resulted in some recrystallization and growth. The crystal structure of aluminum is face-centered cubic (FCC), with four equivalents < 111 > crystallographic directions. Reflecting

the preferred crystallographic orientation of the grains in the sample, the pole figure exhibits intensity peaks along the < 111 > directions. It appears that sonotrode-applied force and movement may affect the texture of aluminum even far from the bonding interface as it caused some specific orientation in the grain's distribution. The IPF map depicts a largely random distribution of small grains, whereas the distribution of larger grains closely resembles that of rolled grains. This distribution pattern could be the result of dynamic recrystallization during the plasticity effect of sonotrode movement. Figure 6b of the Cu110 EBSD-IPF image depicts preferentially oriented crystals. Although some small-sized grains are visible in the middle of the figure (narrow line), the SEM image demonstrates that these are printing process defects, which appear as black areas in the SEM image. Since the particle size in the upper and lower areas of this dark region is unaltered, this dark region could not have resulted from the UAM process. According to the IPF image, the particle orientation and sizes do not exhibit any recrystallization or unexpected localized plasticity, which is consistent with the previously mentioned mechanical properties of strength and the higher surface hardness of copper compared to aluminum (the results of Young's modulus and hardness will describe in the next section of this paper). Consequently, the copper surface would interact with the aluminum surface to form the bonded interface, whereas the area distant from the interface would not undergo plastic deformation or recrystallization.

Fig. 6 a IPF and pole figure of Al layer after UAM process, which shows a very smooth tendency to < 111 > even far from the interface. **b** IPF and pole figure of Cu110 after UAM process with preferred orientation and some internal printing defects
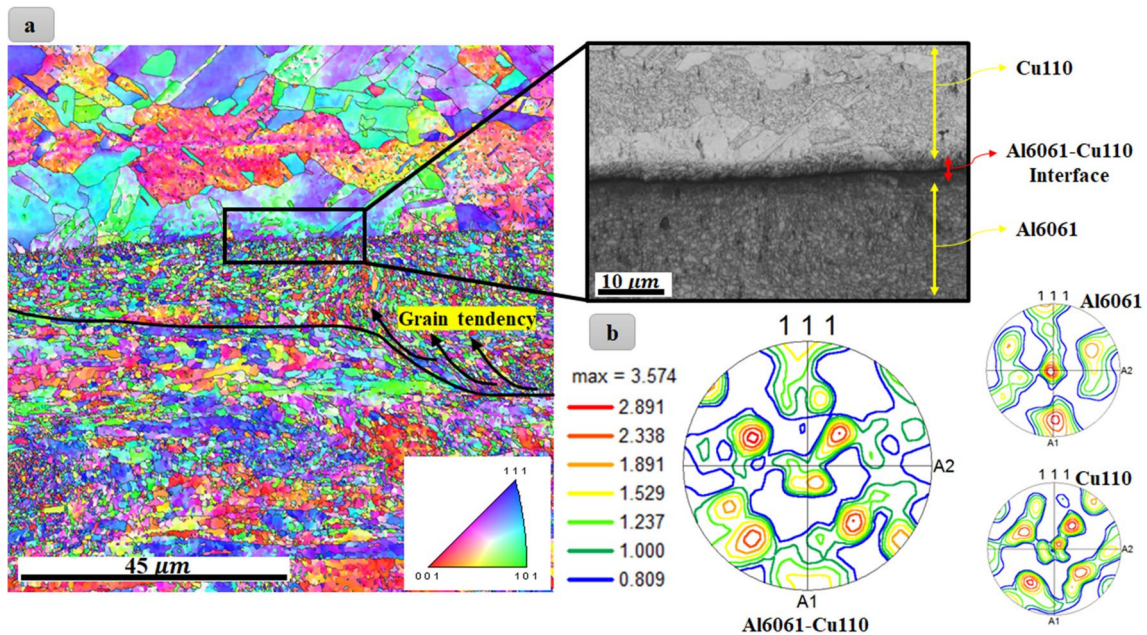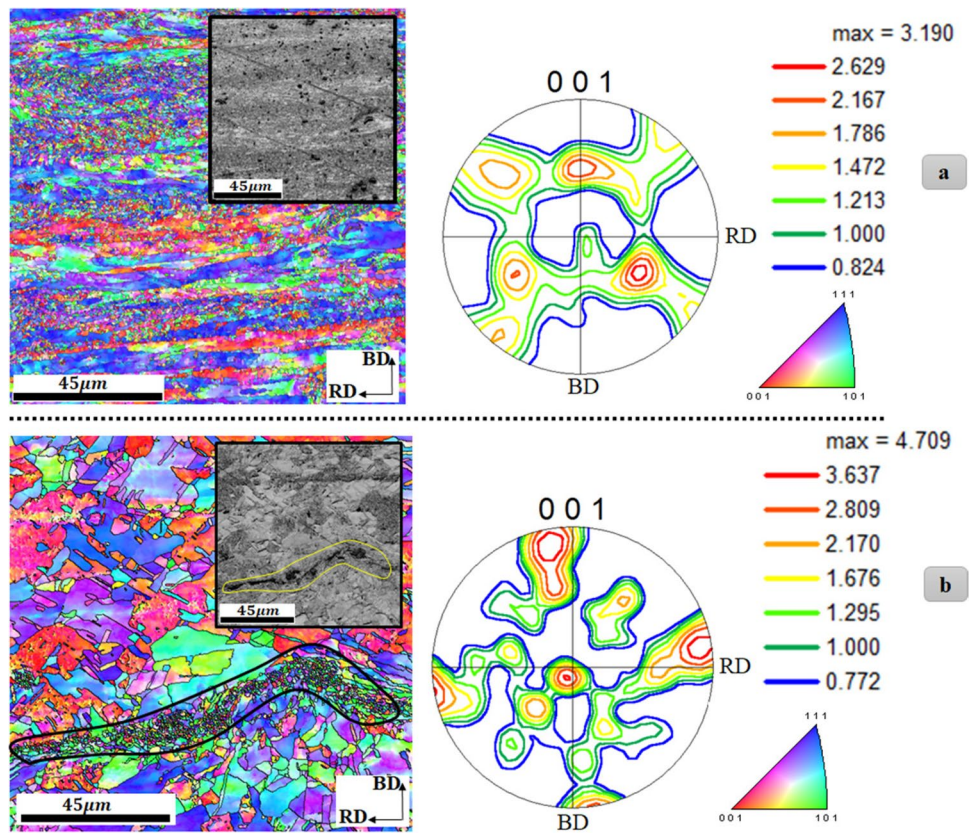

Fig. 7 a The IPF of Al6061-Cu110 layers including the bonded interface. **b** The pole figure of three separated regions of Al6061-Cu110 bonded layers, Al6061, and Cu110 layers based on [111] plane stereograph

3.2.3 Microstructure evolution in the Al-Cu interface

The IPF and pole figure of the bonded Al6061-Cu110 layer (Scan 3 region in Fig. 4) has been represented in Fig. 7, as shown in Fig. 7a, the interface of Al6061-Cu110 does not exhibit any discontinuities, such as porosities, at least on a scale of 45 μm, which is one of the most significant aspects of this research. Due to the distinct mechanical properties and plasticity intensities of these two metals, the IPF image reveals an obvious distinction in grain size between the two interface sides. Figure 7 depicts extreme recrystallization and mass flow trend lines near the interface of Al6061, whereas there is no significant microstructural change on the Cu110 side. Recrystallization in metals such as copper and aluminum is influenced by factors like temperature, the degree of prior deformation, and the presence of impurities [43]. Generally, aluminum, with a higher stacking fault energy (~ 140 mJ/m^2), tends to recrystallize more readily than copper, with comparatively lower stacking fault energy (~ 70 mJ/m^2), at moderate to high temperatures, especially during processes like recovery [44–46]. However, the rate and ease of recrystallization for both aluminum and copper can vary depending on the specific conditions, such as the amount and type of deformation applied, the initial grain size, and the alloying elements or impurity present. The detailed kinetics of recrystallization are complex and are often described by models that take into account the changing microstructural factors and the relationship between the growing grains and the deformed matrix [47].

The laminar grains in the Al6061 far from the interface were discussed in the preceding section, and Fig. 7 displays the same structure. Fuji et al. [36] reported that after the establishment of micro-bonds between aluminum (Al) and copper (Cu), an intense shear deformation occurred in parallel with the ultrasonic vibrations. This process led to the creation of a recrystallized microstructure featuring a shear texture aligned with the $\{111\}\langle011\rangle$ orientation near the bonded interface. The pole figure of the bonded Al6061-Cu110 layer is shown in Fig. 7b. In Fig. 7b, the pole figure of bonded layers is most analogous to the Cu110 pole figure, but it also exhibits some Al6061 pole figure characteristics. It appears that the Al6061 structure is a bit textured as the $<111>$ planes are oriented toward the poles and parallel to the poles. It seems there is a more random texture at the interface (safe to say relatively texture-less). Nevertheless, the intensity is not high.

3.3 Indentation-driven mechanical properties

In Fig. 8, indentation load-depth curves are presented for Al6061-H18 and Cu-110 foils, as well as the substrate (Al6061-T51) at a constant indentation load (300 mN), the Al6061-H18 foil exhibited notably greater indentation depth than the Cu-110 foil, while the substrate showed the shallowest depth. This suggests that the Al6061-H18 foil is softer than the Cu-110 foil, and both foils are softer than the substrate. Indentation depths were measured as 4030 nm, 3426 nm, and 3160 nm for Al6061-H18 foil, Cu-110 foil, and the substrate, respectively. In Fig. 9, we can observe an additional load-depth curve, which pertains to the indents positioned in proximity to the interface and those positioned at a distance from it on Al6061-H18 foil. Examining Fig. 9, it becomes evident

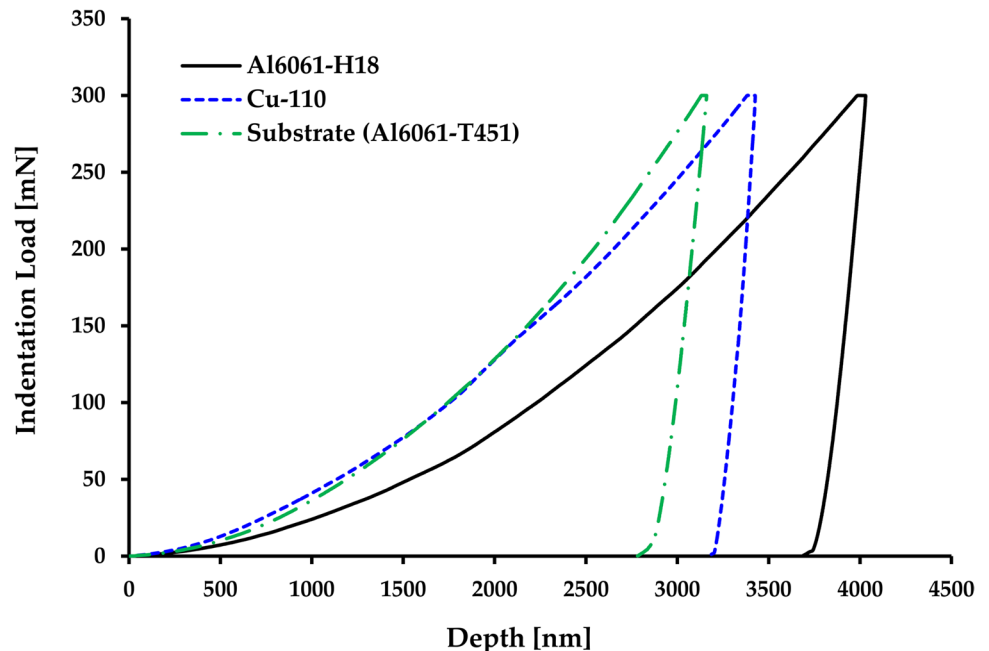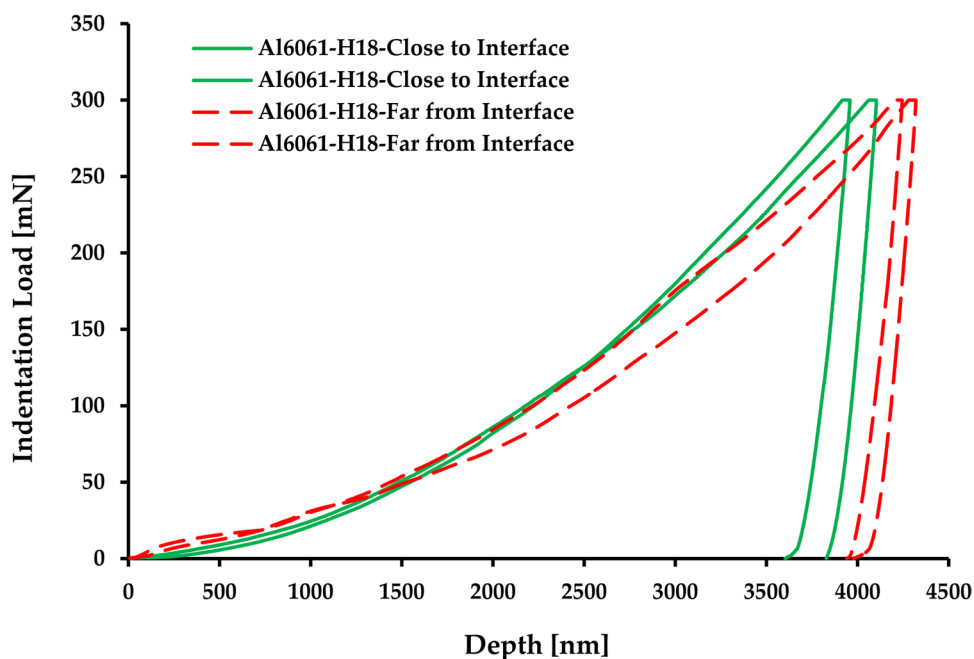**Fig. 8** Representative load-depth curves obtained from depth-sensing nanoindentation tests

Fig. 9 Load-depth curves obtained from Al6061-H18 foil for indents close to the interface and far away from the interface

that the material situated further from the interface exhibits a marginally lower level of hardness, as indicated by the greater indentation depth.

3.3.1 Work hardening, dislocation density, and intermetallic compounds

According to the investigation by Sridharan et al. [15, 17] on steel-Ta and Al-Ti, the cause of the variation of hardness profile on the aluminum part (from the interface to the interior) may be a work-hardening process. Therefore, the variation in hardness (as seen in Fig. 9) can be related to work hardening and corresponding grain size distribution in regions close to the interface and far away from the interface (on the aluminum part). As depicted in Fig. 10, the EBSD findings reveal a notable alteration in the grain size distribution near the interface compared to regions far away from the interface. Although the Cu and Al foils contain some fine grains, it is a characteristic of the interface region. To give a quantitative insight into the fine grain distribution (see Fig. 10c), grains smaller than 3 μm are considered from the Cu, Al, and interface zone. As seen, grains smaller than 3 μm have much higher area fraction in the interface region (shown as gray bars in Fig. 10c) compared to Cu and Al foil. Such fine grain distribution in the interface region can be related to work hardening phenomena in this zone using Hall–Petch relationship [48]:

$$\sigma_y = \sigma_0 + \frac{K}{\sqrt{d}} \tag{1}$$

Through Tabor's theory, nanoindentation hardness, H, can be related to yield stress; therefore, Eq. 1 can convert to Eq. 2:

$$H \propto \frac{1}{\sqrt{d}} \tag{2}$$

where hardness will change linearly with $1/\sqrt{d}$.

EBSD analysis has unveiled that, in the region distant from the interface, Al's grain size distribution comprises 57% of grains measuring less than 3 μm. In contrast, this percentage escalates to approximately 78% as it approaches the interface, signifying a progressive reduction in the average grain size, as illustrated in EBSD images (Fig. 10). Consequently, as the average grain size decreases, the hardness increases following Eq. 2, and this is experimentally observed in Fig. 10. Therefore, the work hardening of aluminum at the interface has been demonstrated using the Hall–Petch theory. Subsequently, equilibrium dislocation density will be calculated using experimental data and the Taylor theory.

An optical micrograph capturing the line of indents performed on the Al-Cu-Al sandwich structure is systematically combined with the nanoindentation results (Vickers hardness and Young's modulus) and EBSD IPF maps (covering interface, Al, and Cu foil microstructure) in Fig. 11. As shown in Fig. 11, the interface microstructure containing fine grains causes a sharp change in the Vickers hardness and Young's modulus with Cu110 material being substantially harder than Al6061. The general trend of these two mechanical properties decreased very slightly with increasing distance
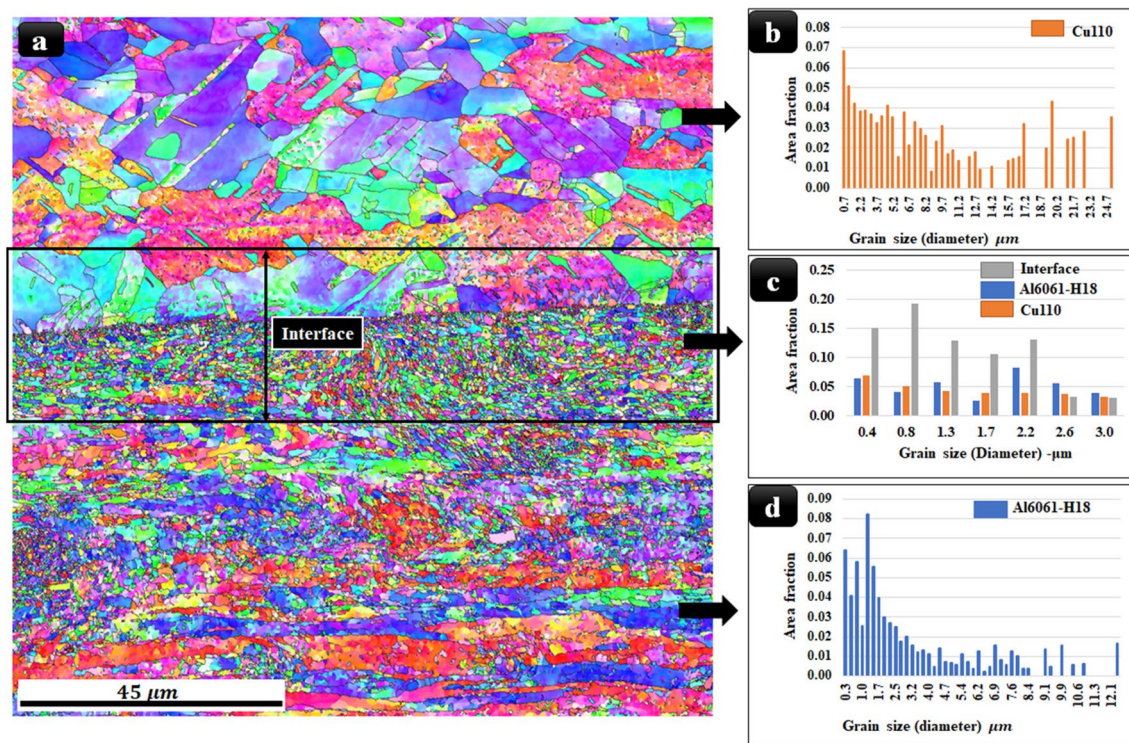
Fig. 10 a EBSD inverse pole figure (IPF) reveals the microstructure at the interface and in regions distant from it, covering both Cu and Al foils, in addition to showcasing the grain size distribution in **b** Cu foil, **c** interface, and **d** Al foil. Note that fine grain distribution with sizes up to 3 μm is considered at the interface and compared with the area fraction of grains up to 3 μm from the Cu and Al foils

Fig. 11 Nanoindentation results for a linear probe from Al6061-Interface-Cu110-Al6061 and reported Vickers hardness and Young's modulus
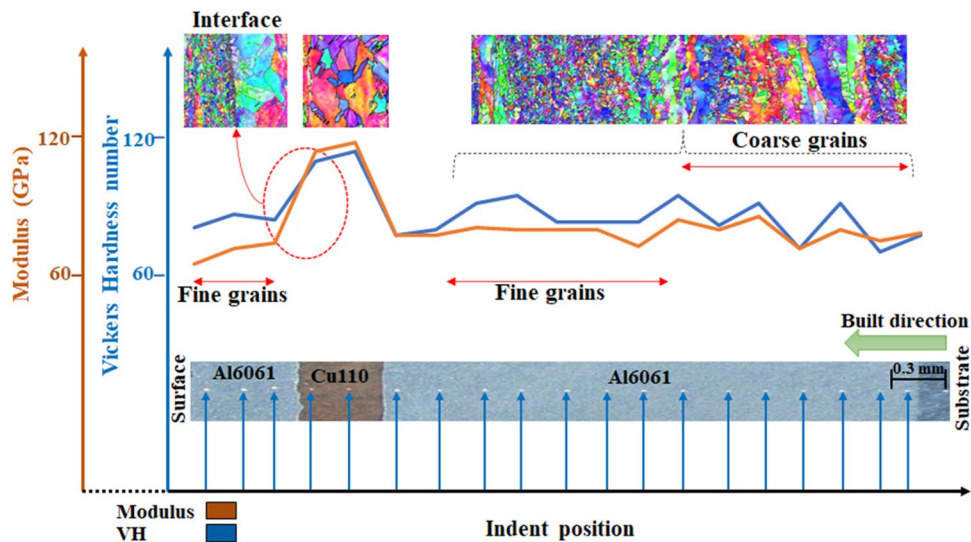

from the Al6061-Cu110 interface, which may be due to the larger grain size in the area far from the interface.

In Fig. 12a, the gradient map of the nanoindentation test shows that Young's modulus diminishes gradually from the interface to the interior area of Al6061. This deduction zone is in the vicinity of the interface with the fine grains' region. On the other hand, most of the plasticity flow was observed on the Al6061 side, whereas Cu110 did not exhibit that much plasticity flow or dynamic recrystallization. Considering the evidence, the phenomena responsible for the sharp change of hardness near the interface are work-hardening phenomena that appear close to interface fine grains. This is due to the interaction of dislocations with the increase in the magnitude of plastic strain. As a dislocation moves

Fig. 12 **a** The nanoindentation map with Young's modulus and hardness gradient map in the Al6061-Cu110 bonded interface, the black circle in the gradient map showing the effect of strain hardening on the beneath interface due to dislocations piling up. **b** The SEM images of Truog et al. [25] and Ikeda et al. [42] studies of intermetallic formation in the UAM and solid bonded interface. **c** The probable intermetallic phases in the interface based on literature and nanoindentation reported data. **d** Schematic illustrations of the bonding process during UAM of Al to Cu and intermetallic formation based on Fujii et al. [36]
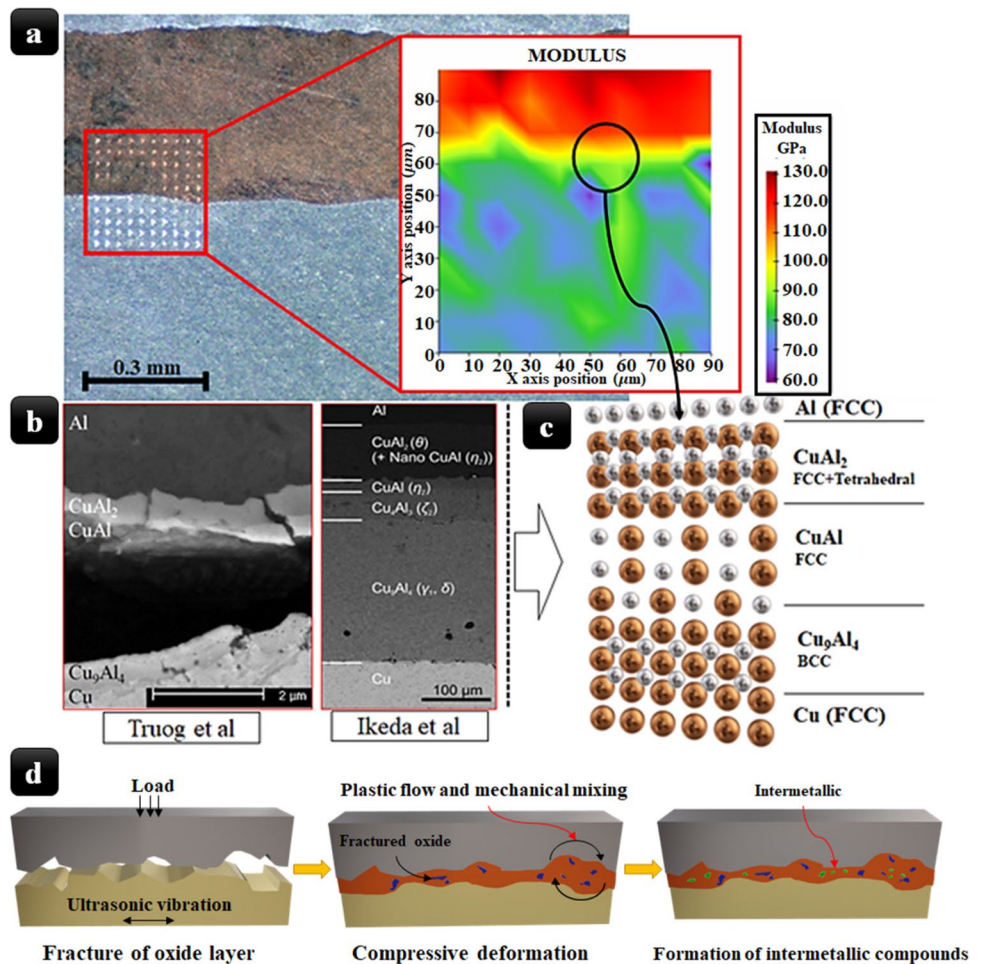
through a stress field, it encounters opposition from other dislocations in the same slip planes. This is represented in a classic Taylor hardening equation (Eq. 3). In this equation, $\Delta\sigma_{sh}$ is the yield strength increase from strain hardening, M is the Taylor factor (3.06 for equiaxed FCC materials), $\alpha \sim 0.1$ [8], G is the shear modulus (26 GPa for Al6061), b is the magnitude of the dislocation Burgers vector, and ρ is the dislocation density [8, 49].

$$\Delta\sigma_{sh} = M.\alpha.G.b.\sqrt{\rho} \tag{3}$$

Using Eq. 4, the magnitude of the Burgers vector in an FCC crystal structure can be calculated based on the lattice parameter of Al6061 (4.049 Å) [8]:

$$b = \frac{a_0}{\sqrt{2}} 110 \tag{4}$$

Therefore, the b for Al would be approximately 2.87 Å. The microstructural characterization of aluminum subjected to UAM deformation [50, 51] indicates a dislocation density between 10^9 and 10^{11} cm^{-2}. Theoretically, the $\Delta\sigma_{sh}$ value for Al could be in a range of 7.2 and 72.2 MPa based on

calculation. On the other hand, Eq. 5 can be used to estimate the increased yield strength around the Al-Cu interface based on the literature concerning the relationship between yield strength and hardness [52, 53].

$$\sigma_y = 3.H_v \tag{5}$$

The average hardness of the area of the fine grain beneath the interface of Al6061 is 83.7 H_V, while the hardness of the interface top point is 106 H_V (Fig. 11). According to Eq. 5, the local yield strength due to strain hardening would be 251.1 MPa beneath the interface and 318 MPa in the interface ($\Delta\sigma_{emperical} = 66.9$ MPa), which is consistent with the calculated $\Delta\sigma_{sh}$ based on the dislocation density ($\Delta\sigma_{Theroritical} = 7.2 - 72.2$ MPa). Consequently, based on theoretical calculations, EBSD images (Fig. 7), and nanoindentation (Figs. 11 and 12a) results, work hardening with a dislocation density of approximately 8.6×10^{10} cm^{-2} occurred beneath the interface. Therefore, work hardening in the interface results in the recrystallization and formation of fine grains while continuing the deformation process by sonotrode.

In addition to work hardening, the formation of intermetallic compounds has also been considered in some studies [16, 29, 30, 42] as a reason behind the elevated hardness near the interface. For instance, in their research on intermetallic phases between Al and Cu, Ikeda et al. [42] reported the following series of intermetallic phases respectively: $Al \rightarrow CuAl_2 \rightarrow CuAl \rightarrow Cu_4Al_3 \rightarrow Cu_9Al_4 \rightarrow Cu$, which are intermetallic phases in the room-temperature bonding processes. Nevertheless, Truog et al. [25] did not record any Cu_4Al_3 at the interface of UAM-bonded specimens, whereas every other intermetallic was detected. Therefore, the change in Vickers hardness and Young's modulus can be influenced by the existence of intermetallics between the Al6061 and Cu110 interfaces. When the findings of Truog et al. [25] are considered, these probabilities become more stringent. Figure 12b shows some findings on intermetallics from the study of Truog et al. [25] and Ikeda et al. [42] while Fig. 12c shows a schematic illustrating a probable atomic arrangement at the interface. However, based on the study of Sietins et al. [37, 54] and some other studies [25, 42], the thickness of intermetallic phases is very thin (less than 10 μm) and it might affect the hardness gradient. Therefore, it might be possible to consider the thin intermetallic phases as the dominant reason behind the sharp change in hardness and Young's modulus, but it needs more investigation for future work. However, a schematic illustration is added in Fig. 12d showing deformation, plastic flow, and intermetallic formation during the bonding process of UAM. At the beginning of UAM, compressive deformation prevails near the bond interface. This, combined with deformation-induced heating, softens the Al alloy, fostering mechanical mixing and plastic flow. As a result, the oxide layer fractures and disperses within the alloy along with Cu particles. Progressing further, shear deformation occurs in the Al alloy and Cu diffusion in Al part eventually forms a metallurgical bond.

4 Summary

The study contributes to the advancement of ultrasonic additive manufacturing (UAM), an advanced manufacturing technique that utilizes ultrasonic vibrations to bond metal foils. By investigating the mechanical properties and changes in the microstructure of the joined interface, the study provides insights into the behavior and performance of UAM-processed metal parts.

In this study, Al6061 and Cu110 foils were utilized in the UAM process to additively manufacture Al-Cu composite structure, and the results demonstrated a significant dependence between material hardness and local plasticity in the UAM process. Near the Al6061-Cu110 bonded interface, substantial plasticity and dynamic recrystallization were observed. The IPF maps and SEM images demonstrated that plasticity flow and recrystallization would only occur near the interface in the softer metal region. While the harder metal did not exhibit any plasticity, mass flow trend, or recrystallization, the hardness and gradient map of Young's modulus indicated the dynamic recrystallization and strain hardening beneath the interface. The hardness values obtained from the nanoindentation hardness map range between the hardness of Cu110 and Al6061 foils, which is close to the values of hardness reported in the literature [8, 15, 17] for the interface zone subjected to strain hardening. Based on the theoretical calculation and the empirical hardness data obtained from this study, the occurrence of strain hardening beneath the interface (in the aluminum area) has been observed, and the probable dislocation density has been calculated close to $8.6 \times 10^{10} cm^{-2}$ that is the main reason for the distribution of fine grains in the thin layer of the interface.

Concerning the potential industrial applications, the conducted research is beneficial for various industries such as aerospace, automotive, and biomedical engineering. UAM offers benefits such as enhanced design flexibility and reduced material waste, making it a promising manufacturing technique for producing complex metal parts. By investigating the mechanical properties and microstructure of UAM-processed Al6061-T451 and Cu-110 foils, the study contributes to the exploration of potential industrial applications for UAM in these industries.

Finally, this study established a significant relationship between material hardness, local plasticity, and microstructural changes in the UAM process. This understanding of material behavior and performance can inform the optimization of UAM parameters, process control, and material selection, leading to improved quality, reliability, and efficiency in the manufacturing of metal parts.

Declarations

Ethics approval Not applicable.

Consent to participate Not applicable.

Consent for publication Not applicable.

Conflict of interest The authors declare no competing interests.

References

1. Zhang H, Senkara J (2011) Resistance welding: fundamentals and applications. CRC press
2. Hehr A, Norfolk M (2019) A comprehensive review of ultrasonic additive manufacturing. Rapid Prototyp J 26(3):445–458
3. Nadimpalli VK, Nagy PB (n.d) Designing an in-situ ultrasonic nondestructive evaluation system for ultrasonic additive manufacturing, AIP Publishing LLC, p. 020005
4. White DR (2003) Ultrasonic consolidation of aluminum tooling. Adv Mater Processes 161(1):64–66
5. White DR (2003) Ultrasonic object consolidation, in: U. patent (Ed.) Solidica, Inc, Ann Arbor, MI, US
6. Ram GDJ, Yang Y, Stucker BE (2006) Effect of process parameters on bond formation during ultrasonic consolidation of aluminum alloy 3003. J Manuf Syst 25(3):221–238
7. Zhou YY, Chen JY, Wang ZQ, Jiang FC (2022) Interfacial texture and bonding strength of Cu/Al laminate metal composite fabricated by ultrasonic additive manufacturing. Sci Technol Weld Join 27(7):501–511
8. Pagan M, Petrie C, Leonard D, Sridharan N, Zinkle S, Babu SS (2021) Interdiffusion of elements during ultrasonic additive manufacturing. Metall Mater Trans A 52:1142–1157
9. Brandt J (n.d) A review of ultrasonic additive manufacturing for particle accelerator applications, pp. 26–29
10. Li D (2021) A review of microstructure evolution during ultrasonic additive manufacturing. Int J Adv Manuf Technol 113:1–19
11. Hehr A, Dapino MJ (2017) Dynamics of ultrasonic additive manufacturing. Ultrasonics 73:49–66
12. Sames WJ, List FA, Pannala S, Dehoff RR, Babu SS (2016) The metallurgy and processing science of metal additive manufacturing. Int Mater Rev 61(5):315–360
13. Han T (2020) Ultrasonic additive manufacturing of steel: process, modeling, and characterization, The Ohio State University
14. Monaghan T, Capel AJ, Christie SD, Harris RA, Friel RJ (2015) Solid-state additive manufacturing for metallized optical fiber integration. Compos A Appl Sci Manuf 76:181–193
15. Sridharan N, Wolcott P, Dapino M, Babu SS (2016) Microstructure and texture evolution in aluminum and commercially pure titanium dissimilar welds fabricated using ultrasonic additive manufacturing. Scripta Mater 117:1–5
16. Wolcott PJ, Sridharan N, Babu SS, Miriyev A, Frage N, Dapino MJ (2016) Characterisation of Al-Ti dissimilar material joints fabricated using ultrasonic additive manufacturing. Sci Technol Weld Join 21(2):114–123
17. Sridharan N, Norfolk M, Babu SS (2016) Characterization of steel-Ta dissimilar metal builds made using very high power ultrasonic additive manufacturing (VHP-UAM). Metall Mater Trans A 47:2517–2528
18. Graff K (2001) AWS Handbook 9th Edition: volume3: Ultrasonic Welding of Metals. American Welding Society
19. Sriraman MR, Babu SS, Short M (2010) Bonding characteristics during very high power ultrasonic additive manufacturing of copper. Scripta Mater 62(8):560–563
20. Fujii HT, Sriraman MR, Babu SS (2011) Quantitative evaluation of bulk and interface microstructures in Al-3003 alloy builds made by very high power ultrasonic additive manufacturing. Metall Mater Trans A 42:4045–4055
21. Sriraman MR, Gonser M, Fujii HT, Babu SS, Bloss M (2011) Thermal transients during processing of materials by very high power ultrasonic additive manufacturing. J Mater Process Technol 211(10):1650–1657
22. Obielodan JO, Stucker BE, Martinez E, Martinez JL, Hernandez DH, Ramirez DA, Murr LE (2011) Optimization of the shear strengths of ultrasonically consolidated Ti/Al 3003 dual-material structures. J Mater Process Technol 211(6):988–995
23. Wolcott PJ, Sridharan N, Babu SS, Miriyev A, Frage N, Dapino MJ (2016) Characterisation of Al–Ti dissimilar material joints fabricated using ultrasonic additive manufacturing. Sci Technol Weld Join 21(2):114–123
24. Hopkins CD, Dapino MJ, Fernandez SA (2010) Statistical characterization of ultrasonic additive manufacturing Ti/Al composites. J Eng Mater Technol 132(4)
25. Truog AG (2012) Bond improvement of Al/Cu joints created by very high power ultrasonic additive manufacturing (Master's thesis, The Ohio State University)
26. Hahnlen R, Dapino MJ, Short M, Graff K (2009) Aluminum-matrix composites with embedded Ni-Ti wires by ultrasonic consolidation. In Industrial and Commercial Applications of Smart Structures Technologies 2009 (vol. 7290, pp. 46–57). SPIE
27. Hahnlen R, Dapino MJ (2014) NiTi–Al interface strength in ultrasonic additive manufacturing composites. Compos B Eng 59:101–108
28. Athar MMH, Tolaminejad B (2015) Weldability window and the effect of interface morphology on the properties of Al/Cu/Al laminated composites fabricated by explosive welding. Mater Des 86:516–525
29. Lee W-B, Bang K-S, Jung S-B (2005) Effects of intermetallic compound on the electrical and mechanical properties of friction welded Cu/Al bimetallic joints during annealing. J Alloy Compd 390(1–2):212–219
30. Wei Y, Li J, Xiong J, Zhang F (2016) Investigation of interdiffusion and intermetallic compounds in Al–Cu joint produced by continuous drive friction welding. Eng Sci Technol Int J 19(1):90–95
31. Johnson K, Edmonds HC, Higginson RL, Harris RA (2011) New discoveries in ultrasonic consolidation nano-structures using emerging analysis techniques. Proc Inst Mech Eng Part L J Mater Des Appl 225(4):277–287
32. Abbasi M, Taheri AK, Salehi MT (2001) Growth rate of intermetallic compounds in Al/Cu bimetal produced by cold roll welding process. J Alloy Compd 319(1–2):233–241
33. Ouyang J, Yarrapareddy E, Kovacevic R (2006) Microstructural evolution in the friction stir welded 6061 aluminum alloy (T6-temper condition) to copper. J Mater Process Technol 172(1):110–122
34. Ram GDJ, Johnson DH, Stucker BE (2007) Ultrasonic consolidation with aluminum and copper. CRC Press, Virtual and Rapid Manufacturing, pp 603–610
35. Sietins JM, Gillespie JW, Advani SG (2014) Transmission electron microscopy of an ultrasonically consolidated copper-aluminum interface. J Mater Res 29(17):1970–1977
36. Fujii HT, Endo H, Sato YS, Kokawa H (2018) Interfacial microstructure evolution and weld formation during ultrasonic welding of Al alloy to Cu. Mater Charact 139:233–240
37. Sietins JM (2014) Exploring diffusion of ultrasonically consolidated aluminum and copper films through scanning and transmission electron microscopy. University of Delaware
38. Li DZ (2021) A review of microstructure evolution during ultrasonic additive manufacturing. Int J Adv Manuf Technol 113(1–2):1–19

39. International Organization for Standardization (2002) Metallic materials: instrumented indentation test for hardness and materials parameters. Test Method. ISO

40. Oliver WC, Pharr GM (1992) An improved technique for determining hardness and elastic modulus using load and displacement sensing indentation experiments. J Mater Res 7(6):1564–1583

41. Zobac O, Kroupa A, Zemanova A, Richter KW (2019) Experimental description of the Al-Cu binary phase diagram. Metall Mater Trans A 50:3805–3815

42. Ikeda Y, Mancias J, Gan B, Maaß R (2021) Evidence of room-temperature shear-deformation in a Cu-Al intermetallic. Scripta Mater 190:126–130

43. Ueki M, Horie S, Nakamura T (1987) Factors affecting dynamic recrystallization of metals and alloys. Mater Sci Technol 3(5):329–337

44. Dillamore IL, Smallman RE (1965) The stacking-fault energy of FCC metals. Phil Mag 12(115):191–193

45. Smallman RE, Dobson PS (1970) Stacking fault energy measurement from diffusion. Metall Trans 1(9):2383–2389

46. Dodaran MS, Guo S, Khonsari MM, Shamsaei N, Shao S (2021) A theoretical calculation of stacking fault energy of Ni alloys: the effects of temperature and composition. Comput Mater Sci 191:110326

47. Lu G, Kioussis N, Bulatov VV, Kaxiras E (2000) Generalized-stacking-fault energy surface and dislocation properties of aluminum. Phys Rev B 62(5):3099

48. Pagan M, Ohmura T, Wang L, Zinkle S, Babu SS (2022) Strengthening effects at dissimilar metal interfaces created by ultrasonic additive manufacturing. Metall Mater Trans A 53(10):3547–3564

49. Dieter GE, Bacon D (1976) Mechanical metallurgy, vol 3. New York, McGraw-hill, pp 43–53

50. Schick DE (2009) Characterization of aluminum 3003 ultrasonic additive manufacturing (Master's thesis, The Ohio State University)

51. Dehoff RR, Babu SS (2010) Characterization of interfacial microstructures in 3003 aluminum alloy blocks fabricated by ultrasonic additive manufacturing. Acta Mater 58(13):4305–4315

52. Khodabakhshi F, Haghshenas M, Eskandari H, Koohbor B (2015) Hardness - strength relationships in fine and ultra-fine grained metals processed through constrained groove pressing. Mat Sci Eng A-Struct 636:331–339

53. Brooks I, Lin P, Palumbo G, Hibbard GD, Erb U (2008) Analysis of hardness-tensile strength relationships for electroformed nanocrystalline materials. Mat Sci Eng A-Struct 491(1–2):412–419

54. Sietins JM, Gillespie JW, Advani SG (2014) Transmission electron microscopy of an ultrasonically consolidated copper–aluminum interface. J Mater Res 29(17):1970–1977